**Naval Research Laboratory**

**Washington, DC 20375-5320**

**NRL/MR/6750--09-9203**

# Plasma-Enhanced Chemical Vapor Deposition of $SiO_x$ Films Using Electron Beam Generated Plasmas

DARRIN LEONHARDT

*Fusion UV Systems, Inc.*
*Gaithersburg, Maryland*

SCOTT G. WALTON

*Charged Particle Physics Branch*
*Plasma Physics Division*

R.T. HOLM

*Power Electronics Branch*
*Electronics Science and Technology Division*

September 28, 2009

# REPORT DOCUMENTATION PAGE

*Form Approved*
*OMB No. 0704-0188*



| **1. REPORT DATE** *(DD-MM-YYYY)* | **2. REPORT TYPE** | **3. DATES COVERED** *(From - To)* |
|---|---|---|
| 28-09-2009 | Memorandum | |

**4. TITLE AND SUBTITLE**

Plasma-Enhanced Chemical Vapor Deposition of $SiO_x$ Films Using Electron Beam Generated Plasmas

**5a. CONTRACT NUMBER**

**5b. GRANT NUMBER**

**5c. PROGRAM ELEMENT NUMBER**

**6. AUTHOR(S)**

Darrin Leonhardt*, Scott G. Walton, and R.T. Holm

**5d. PROJECT NUMBER**
67-9870-09

**5e. TASK NUMBER**

**5f. WORK UNIT NUMBER**

**7. PERFORMING ORGANIZATION NAME(S) AND ADDRESS(ES)**

Naval Research Laboratory
4555 Overlook Avenue, SW
Washington, DC 20375-5320

**8. PERFORMING ORGANIZATION REPORT NUMBER**

NRL/MR/6750--09-9203

**9. SPONSORING / MONITORING AGENCY NAME(S) AND ADDRESS(ES)**

Office of Naval Research
One Liberty Center
875 North Randolph Street
Arlington, VA 22203-1995

**10. SPONSOR / MONITOR'S ACRONYM(S)**

ONR

**11. SPONSOR / MONITOR'S REPORT NUMBER(S)**

**12. DISTRIBUTION / AVAILABILITY STATEMENT**

Approved for public release; distribution is unlimited.

**13. SUPPLEMENTARY NOTES**

*Fusion UV Systems, Inc., 910 Clopper Road, Gaithersburg, MD 20878

**14. ABSTRACT**

Tetraethyl orthosilicate (TEOS) was used as a silicon source to grow $SiO_2$ films in a modulated electron beam generated plasma enhanced chemical vapor deposition (PECVD) arrangement. Process parameters investigated were: substrate temperature, gas composition, duty factor, and incident ion energy. At high temperatures (> 150 °C), film compositions were less sensitive to the process parameters, while at lower temperatures, the film chemistries varied greatly. Activation energies of –0.122 eV and –0.020 eV were determined for the films grown in these respective temperature ranges. Below 250 °C, preferred growth conditions (> 20 nm/min) were found at small flow percentages of TEOS in argon/oxygen mixtures (2:48:50) with increased ion energies. The trade-off between substrate temperature and incident ion energy demonstrated a process viability not previously seen in scalable PECVD systems.

**15. SUBJECT TERMS**

Electron beam produced plasmas
Deposition
PEVCD
SIO

| **16. SECURITY CLASSIFICATION OF:** | | | **17. LIMITATION OF ABSTRACT** | **18. NUMBER OF PAGES** | **19a. NAME OF RESPONSIBLE PERSON** |
|---|---|---|---|---|---|
| | | | | | Scott G. Walton |
| **a. REPORT** | **b. ABSTRACT** | **c. THIS PAGE** | UL | 25 | **19b. TELEPHONE NUMBER** *(include area code)* |
| Unclassified | Unclassified | Unclassified | | | (202) 767-7531 |

**Standard Form 298 (Rev. 8-98)**
**Prescribed by ANSI Std. Z39.18**

## CONTENTS

## I. INTRODUCTION

Silicon dioxide ($SiO_2$) films have been used for many years for their dielectric and barrier properties. The deposition of scalable high-quality films requires large fluxes of chemically active particles that have been provided by various deposition schemes. While physical vapor deposition, electron beam evaporation, ion beam assisted deposition or sputtering have been used industrially for many years to produce films, higher deposition rates, better process optimization, improved conformal coverage and uniformity are typically achieved in plasma-based deposition environments [1]. Plasma enhanced chemical vapor deposition (PECVD) [2,3] remote PECVD (RPECVD) [4] and magnetron sputtering [5] have all produced films of various qualities, depending on the plasma source and application, with respect to chemical purity, process viability and scalability. While improvements in film quality can be made using the more versatile PECVD arrangements, incident ion energies and the flux of critical species are difficult plasma parameters to tune ad hoc. Ion energy is well known [6,7] to densify films especially at lower process temperatures, but additional ion energy can also damage the final film. The significance of these effects will clearly depend on the particular application, which has been discussed at length in the scientific literature. Thin film transistors (TFTs) required for the growing flexible electronics applications require high-quality, impermeable silicon dioxide [8] or silicon nitride (SiN) [9,10] dielectric layers as well as amorphous [11,12] or polycrystalline [13] silicon semiconductor layers deposited at low temperatures to preserve the integrity of the organic substrates (i.e. polycarbonate, polyethylene terephthalate/naphthalate). The dielectric layer tends to be the critical stop-gap in the fabrication of TFTs, since the barrier and electrical properties degrade rapidly with decreasing deposition temperature [14]. In addition to TFTs, plastic substrates have been actively replacing glass in many optical systems, from single-element lenses to multiple-square meter architectural glazings [15]. These 'safer substrates' coated by dielectric films with tailor-made indices of refraction offer better mechanical properties and are far better suited for roll-to-roll processing than their traditional glass counterparts.

Electron beams have been used to create low temperature, non-equilibrium plasmas for materials modification in a variety of arrangements. Thompson et al. [16] developed electron beam sources to supply 50-450 $mA/cm^2$ beam currents in moderate pressure (0.1 to 1 Torr) regimes, then Rocca et al. [17] applied these sources to deposit $SiO_2$ films, under various beam conditions. Later, Schatz and Ruzic [18] then Kushner et al. [19] used an electron beam as a secondary ionization source in a capacitively coupled reactive ion etching system to increase control over incident ions. At NRL, a large area plasma processing system (LAPPS) was developed [20] based solely on the ionization by a high energy (multiple kilovolt) electron beam. These systems have been developed for use over wide operating ranges including low beam currents (~ 1 $mA/cm^2$), with an emphasis on the actual plasma generation [21,22] and subsequent control of specie flux to surfaces [23,24]. Systems utilizing small diameter (< 1 $cm^2$) pencil-like electron beams to half-meter wide sheet electron beams have been demonstrated with high consistency and simplicity.

In this work, a scalable PECVD process for $SiO_2$-like films from an electron beam generated plasma is discussed. Tetraethyl orthosilicate (TEOS) was used as the silicon precursor to circumvent handling problems associated with silane. Similar to our previous work [25,26], the emphasis here is on the unique properties of the plasma being generated and the requirements for improved process control. Basic process variables (gas composition,

Manuscript approved August 28, 2009.

duty factor, surface temperature, incident ion energy) were adjusted and correlated to the final films' growth rate, chemical composition, smoothness, and porosity. Because of the low plasma potentials (≤ 5 V) of these systems, a wider tuning range of incident ion energies was available from an externally applied rf bias. A lower energy limit was established to produce stable films at 200 °C deposition temperatures.

## II. EXPERIMENTAL

The system used in the present experiments was identical to previous work [27] so only details specific to the PECVD process are emphasized here. A 1x25 $cm^2$ electron beam (e-beam) was generated by a hollow cathode energized with a -2 kV pulse for a duration of 2 ms at a 10 ms period (20% duty factor typical). The beam immediately passed through a slotted anode at ground potential then traveled approximately 40 cm before terminating in to the end of the vacuum chamber. A 165 G magnetic field from an external pair of Helmholtz coils collimated the beam over the length of the chamber. The chamber was ≈ 50 cm in diameter and 56 cm long with a base pressure < $10^{-6}$ Torr provided by a 500 l/s turbomolecular pump. Figure 1 shows the arrangement of the chamber for the present experiments. Process pressures were measured with a capacitance manometer gauge.

Substrates were half-wafers of 5 cm diameter p-type <100> silicon (resistivity 1-20 Ω-cm). These substrates were chosen because of their reasonable transparency in the IR. Samples were dipped in a 5% HF solution, immediately mounted on the processing stage and placed in vacuo, 2.5 cm from the edge of the electron beam. The front of the substrate stage was an electrically isolated 14 cm diameter copper plate and the body contained an internal heater and thermocouple. This internal thermocouple was calibrated against the actual sample surface temperature of a sacrificial substrate. The substrate was held to the copper plate by ceramic clips at opposite edges. TEOS was introduced by flowing 10 sccm of argon through a room temperature bubbler kept at 18 Torr by a throttle valve between the bubbler and a 0.64 cm diameter gas feed tube that extended to the stage surface next to the sample. Argon (40 sccm) and oxygen (50 sccm) were introduced through the system sidewall with no special relation to the substrate or e-beam. A total flow of 100 sccm was used in all cases. For the gas flows mentioned above, the individual flows were calculated to be 2/48/50 sccm of TEOS/Ar/O2, respectively. These flows and the 20% duty factor were the standard conditions used in experiments. Exposure time was the total time

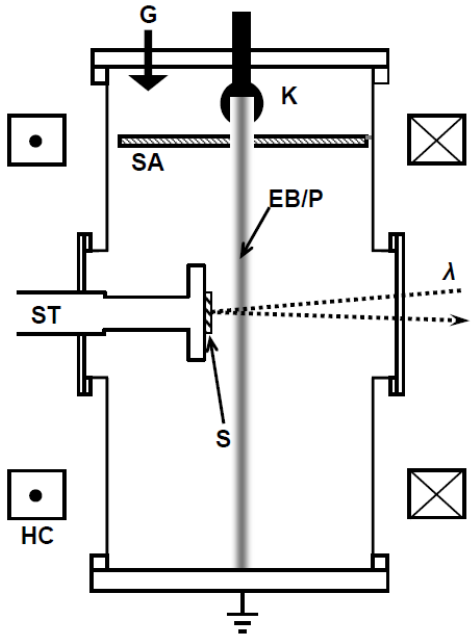


**Fig. 1** Schematic of experimental system. System components are labeled as: (K) hollow cathode beam source; (G) $Ar/O_2$ gas feed; (EB/P) sheet electron beam and plasma; (S) substrate; (ST) stage body; (SA) slotted anode; (HC) Helmholtz coils; (λ) reflectometer laser beam. TEOS gas feeds, gauges and pumps were omitted for clarity.

that the plasma was on; thus the actual (laboratory) time would be the exposure time divided by the duty factor (0.2 for standard conditions). For most films, the exposure time was approximately 35 minutes.
The TEOS reservoir was degassed before each growth and the precursor gas line was heated to prevent condensation. The substrate temperature was reached in approximately 20 minutes and then equilibrated for another 15 minutes before a pretreatment plasma (20% duty factor, 50 sccm each of Ar and O2) was run for 4-5 minutes of exposure time. For deposition, the TEOS/Ar/O2 gas flows were adjusted accordingly, which increased the operating pressure from 52 mTorr to approximately 55 mTorr. A HeNe (632.8 nm) reflectometer monitored the film growth in situ. After the deposition, a plasma post-treatment identical to the pre-treatment was carried out.

To increase the incident ion energy, rf (13.6 MHz) power was applied through a capacitively coupled rf network, to form an rf-induced, dc bias on the stage front. The rf power was synced to the e-beam pulse width. For these experiments it was necessary to reconfigure the TEOS gas line to minimize parasitic rf couplings. The precursor delivery tube directly above the stage was replaced by two tubes that introduced gas at opposite sides of the stage perimeter. The applied peak-to-peak rf voltage ($V^{rf}_{pp}$) was measured at the stage power feedthrough with an oscilloscope 10X probe and was kept constant during deposition. The rf power was also measured with directional couplers. During the pre/post treatment phases of the ion energy experiments, an $V^{rf}_{pp}$ of 50 V was set as the standard condition. No etching was detected by the reflectometer during the post-treatment phase.

After the plasma post-treatment, the stage heating or cooling was turned off and the sample was allowed to come to room temperature. The sample was removed from vacuum and the film thickness was measured with a white-light spectrophotometer and/or profilometry, after a wet etch of a partially masked (Shipley 1818) portion of the sample. The compositions of the resultant films were analyzed by FTIR (Nicolet Magna 750 set at 4 cm-1 resolution; MCT detector) and the spectra were not normalized for the variation in film thickness. To compare steady-state film compositions [28,29], FTIR analysis shown here was carried out after at least a week of exposure to laboratory air. All spectra were referenced with respect to a clean substrate. Wet etching in a ‘P etch’ solution [30] of $15HF:10HNO_3:300H_2O$ (by volume), atomic force microscopy (AFM), single-wavelength (632.8 nm) ellipsometry, and breakdown field measurements were also done ex situ on the films. Gold contacts (1.5 mm diameter, 300-500 nm thick) were deposited on samples of various incident ion energies to measure capacitance–voltage (CV) characteristics of the resultant metal-oxide-semiconductor (MOS) capacitor structure. The flatband voltage ($V_{FB}$) was determined by the gate voltage that reduced the oxide capacitance to 96% of its full accumulation value at a 100 kHz dither frequency. This percentage was determined from Eqn. 6.12 in [31] for the silicon substrates used.

Flux composition and ion energy distributions were determined using a differentially pumped Hiden EQP300 quadrupole mass spectrometer with tandem energy analyzer as discussed in [32]. Ions from plasma gas mixtures containing 0% and 2% TEOS were sampled through a 100 micron orifice in the center of a grounded stainless steel electrode located 1.2 cm from the beam edge. Ion flux measurements were time resolved with standard gating techniques over a 3 ms window that included the entire e-beam pulse and 1 ms of the afterglow. Mass and energy resolutions were 0.2 amu and 0.15 eV, respectively; spectra were not corrected for mass transmission efficiencies. Neutral species were sampled with the same

apparatus, however the front electrostatic lens element in the spectrometer was positively biased to exclude plasma ions and the ionizer filament was run continuously at a potential of 70 V. Neutral mass spectra were collected from the plasma gas mixtures containing both 0% and 50% oxygen with the e-beam run at the 20% duty factor. All neutral species were acquired continuously, with no correlation to the e-beam pulse. For comparison, neutral mass spectra were also taken with the plasma source off.

## III. RESULTS

### A. Ion flux and energy distributions

The ion current to the stage was estimated to be ≈ 0.44 mA during the plasma pulse. The ion energy distribution functions (IEDFs) for the dominant ions in the 50/50 mixture of argon and oxygen are shown in Fig. 2. The measured distributions have main peaks centered at 1.25 eV with FWHM < 0.5 eV, and possess various high and low energy tails. It should be noted that while these IEDFs might exhibit some instrument broadening, the majority of the distributions result from time-dependent plasma phenomena. The $Ar^+$ ion distributions appeared the most symmetric, with an extended high energy portion while the $O_2^+$ ion distributions contained a low energy shoulder at approximately 0.9 eV and a tail out to 3.0 eV. The $O^+$ ion distribution similarly contained a high energy tail. The complete ion flux mass spectrum for the $Ar/O_2$ mixture and the standard deposition gas mixture 2/48/50 of $TEOS/Ar/O_2$ are shown in Fig. 3. Identification of species with respect to the mass-to-charge ratio (m/q) was considered straightforward, or is further discussed in Section IV(a). In the absence of TEOS, the most pronounced ions scaled to the dominant $O_2^+$ ion peak were $Ar^+$ (37%) and $O^+$ (19%). The gas mixture containing TEOS continued to show $O_2^+$ as the dominant ion at the surface, but the other abundant ion species were observed at m/q = 19 ($H_3O^+$ at 50%), 18 ($H_2O^+$ at 27%), 29 ($C_2H_5^+$ or $COH^+$ at 20%) and 40 ($Ar^+$ at 19%). The higher mass portion (intensity increased by a factor of 100) is shown in the inset of Fig. 3.

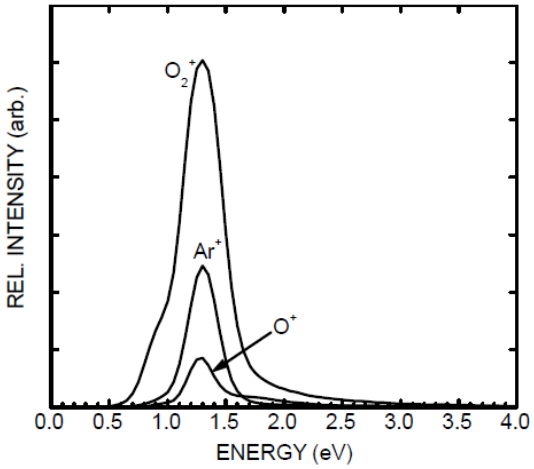


**Fig. 2** Ion energy distribution functions measured 1.2 cm from the edge of an $Ar/O_2$ e-beam generated plasma.

The neutral spectra were extremely rich with structure. However, since an absolute calibration was not possible, only global spectra comparisons and relative changes in peaks with respect to the plasma operation will be provided here. All distributions were normalized to the $Ar^+$ intensity; changes in $Ar^+$ from one measurement to the other are indicative of system drift and/or slight changes in system operation. In all gas mixtures, the higher mass peaks ($64 \leq m/q \leq 208$) associated with TEOS were dramatically reduced when the plasma was present. In the oxygen-free gas mixture, mass peaks corresponding to m/q = 26 ($C_2H_2^+$), 28 ($CO^+$, $C_2H_4^+$) and 2 ($H_2^+$) showed the most notable changes (peaks at the 1% level), increasing by a factor of 2 to 5. In the presence of plasma, less pronounced peaks (< 0.1%)

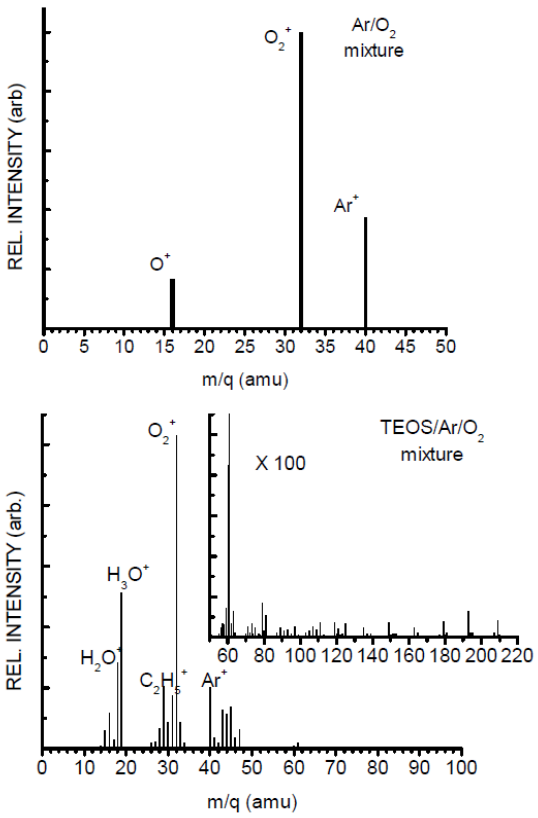


**Fig. 3** Ion mass spectrum of $Ar/O_2$ plasma (top) and $TEOS/Ar/O_2$ plasma (bottom).

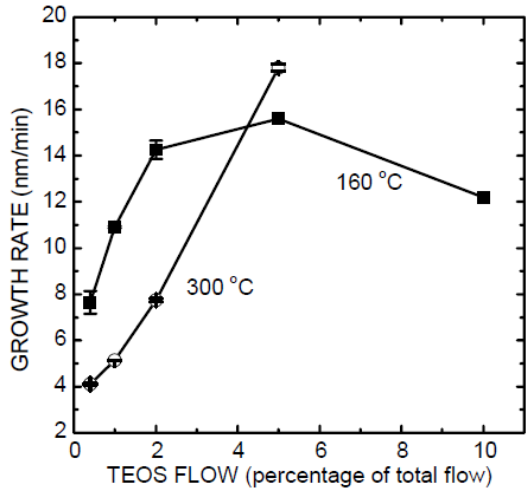


**Fig. 4** Growth rate of films with various TEOS flows at substrate temperatures of 160 °C (solid symbol) and 300 °C (open symbol). Argon was used as the balance gas; oxygen flow was kept constant.

appeared: m/q = 78 ($Si(OH)_2O^+$), 50 ($SiH_3OH^+$, $H_2O_3^+$) and 56 ($Si_2^+$, $SiOC^+$, $C_2O_2^+$). In the standard gas mixture containing oxygen, the molecular oxygen peak decreased by over 20% while a number of ions (appearing at the 1 to 10% level) roughly doubled in intensity. In order of abundance, these species had m/q values of 28 ($CO^+$, $C_2H_4^+$), 18 ($H_2O^+$), 44 ($CO_2^+$, $C_2H_4O^+$, $SiO^+$), and 2 ($H_2^+$).

## B. Gas composition and duty factor dependence

In order to determine the initial viability of $SiO_x$ PECVD in this system, the stage was electrically grounded and the substrate temperature was fixed while the gas flows and duty factor were varied. Figure 4 shows the deposition rate of films with respect to the TEOS flow rate at 160 and 300 °C. In these tests, the $O_2$ flow was kept at 50 sccm while the argon flow through the TEOS reservoir was varied and balanced with the pure argon flow to maintain a total flow rate of 100 sccm. The reported error bars refer to thicknesses taken at various locations of the sample, as in all data presented here. At 160 °C the growth rate maximized at 5 sccm TEOS flow, while at 300 °C the growth rate appeared to continually increase. The lowest measured wet etch rate for these films was 89 nm/min for the film grown at 300 °C and 2 sccm TEOS flow. The etch rate for all of the other films was over 130 nm/min, although at low TEOS flow the samples were very thin and precise etch rate determinations were difficult. The index of refraction (n) and breakdown fields ($E_{BD}$) of these films decreased linearly (1.4533 to 1.4340 and 12 to 6.5 MV/cm, respectively) with the TEOS flow. Overall, well-adhered highly specular films were grown on the silicon substrates in all of the deposition experiments, although white particulates loosely formed on the

chamber surfaces that were not in close contact with the plasma.

The FTIR spectra for the films grown at 300 °C are shown in Fig. 5. Following the identification scheme of previous workers [33], typical Si-O-Si peaks (stretching at 1070 $cm^{-1}$ with the high energy shoulder, bending at 812 $cm^{-1}$ and rocking at 450 $cm^{-1}$) were present in all films as well as SiO-H stretching (3650 and 3450 $cm^{-1}$) at the higher TEOS flow rates. Since minor changes in peak position and width are dependent on many factors including film thickness and position in spectrometer, such analyses were not carried out. However, it should be noted that the position of the Si-O-Si peaks remained within 4 $cm^{-1}$ of one another for each series of experiments.

The oxygen flow was varied with a constant 2 sccm flow of TEOS and an argon balance to maintain the 100 sccm total flow rate. With the stage grounded and at 300 °C, the initial presence of oxygen in the feedstock gas rapidly increased the film growth rate as well as reduced the chemical etch rate, although there was no strong dependency among the mixtures that contained $O_2$ (see Fig. 6). Similarly, the film grown without any additional oxygen showed the lowest index of refraction and $E_{BD}$ values (1.4340 and 6.9 MV/cm, respectively), which then varied from 1.4583 to 1.4566 and 9.5 to 7.5 MV/cm for the mixtures containing oxygen. The FTIR spectra of these films are shown in Fig. 7. In addition to the Si-O-Si peaks and silanol (SiO-H) peaks identified previously, another silanol peak (SiO-H bend) appeared in these films at 933 $cm^{-1}$ and an aliphatic chain presence (C-H stretch at 2950 $cm^{-1}$) appeared at the 0% $O_2$ growth condition.

The plasma duty factor was varied with the standard gas mixture (2/48/50 sccm), grounded stage and 300 °C

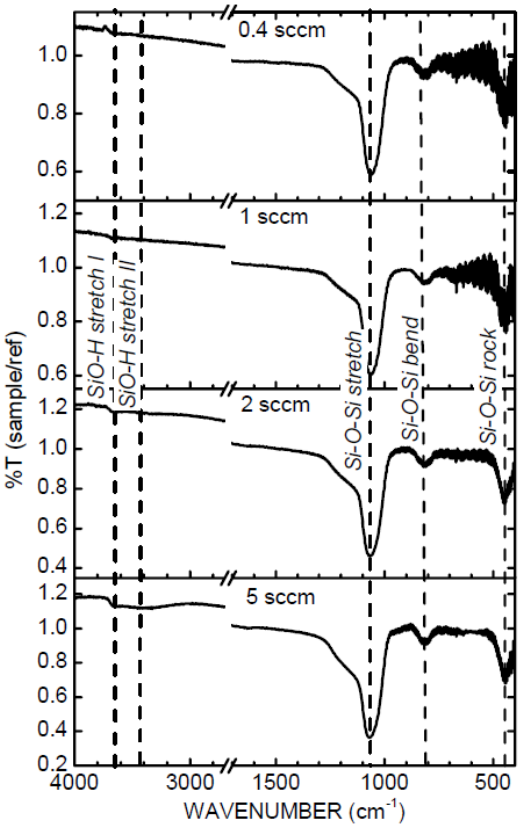


**Fig. 5** FTIR spectra of films grown at various TEOS flow rates. Dotted lines mark peak positions discussed in the text.

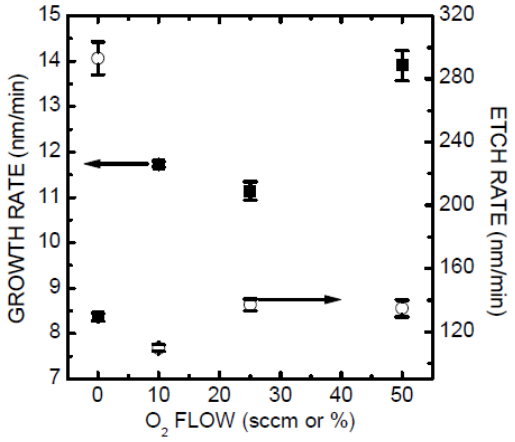


**Fig. 6** Growth (solid) and etch (open) rate variation with oxygen flow. Argon was used as the balance gas; TEOS flow was kept constant.

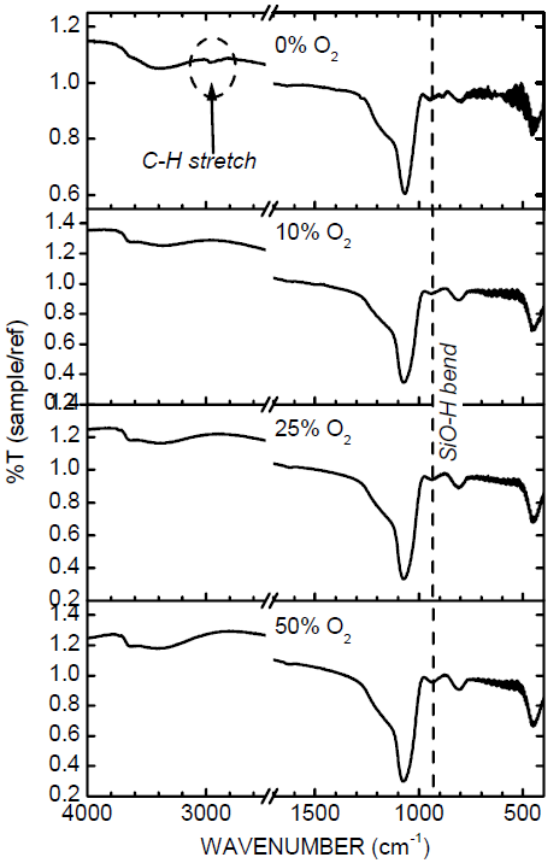


**Fig. 7** FTIR spectra of films grown at various oxygen flow rates. Dotted lines mark peak positions discussed in the text.

substrate temperature. The variation in duty factor was obtained by changing the period of the 2 ms plasma pulse. Fig. 8 shows the growth and etch rates with respect to the duty factor. Both rates rapidly dropped as the duty factor increased from 0% to 20%. The index of refraction and EBD varied independent of the duty factor (1.4399 to 1.4552 and 5.1 to 8.7 MV/cm, respectively), however high n values were observed with low $E_{BD}$ values and vice versa. The FTIR spectra showed nearly identical compositions, with the aforementioned Si-O-Si and SiO-H bonding peaks.

### C. Temperature dependence

The temperature of the substrates was varied at the standard gas flow rates and duty factor with the stage grounded for nearly constant exposure times. The dependence of the growth and etch rates on the substrate temperature are shown in Fig. 9. Both rates decreased linearly with temperature although the etch rate changed abruptly below 100 °C. An Arrhenius-type plot constructed from the growth rate data (Fig. 9, bottom) resulted in a two distinct lines with positive slopes above and below 150 °C. The activation energies for the PECVD process in these respective temperature ranges was -0.122 eV and -0.020 eV. The FTIR spectra for some of the films are shown in Fig. 10. As the deposition temperature decreased, the films showed an increased presence of silanol groups (increased 3450 $cm^{-1}$ peak). When the deposition temperature dropped below 200 °C, the additional silanol peak at 933 $cm^{-1}$ also became more pronounced. As the deposition temperature continued to decrease, peaks at 1712 $cm^{-1}$ (C=O stretch), 3250 and 1600 $cm^{-1}$ (HO-H stretch/scissor) appeared as the amplitudes of the silanol peaks increased. The films grown at lower temperatures were brownish in color and approximately one micron thick; the index of refraction measurements were erratic (1.4432 to 1.4656) with the deposition temperature although $E_{BD}$ went from approximately 5 MV/cm at low temperatures to 10 MV/cm at the higher temperatures.

### D. Ion energy dependence

The position variation of the TEOS gas feed showed little effect on the film growth rate or composition. The effects of ion energy on the film growth and composition were determined with the substrate temperature fixed at 200 °C while the plasma gas composition

**Table 1:** RF signal measurements for a biased stage and the resultant film roughness, breakdown field ($E_{BD}$), and flatband voltage ($V_{FB}$) of MOS capacitors.

| $V^{rf}_{pp}$ (V) | $< V^{rf}_{pp} >$ (V) | Power (mW/cm$^2$) | RMS roughness (nm) | $E_{BD}$ (MV/cm) | $V_{FB}$ (V) |
|---|---|---|---|---|---|
| 100 | -47 | 147 | 0.346 | 13.7 ± 3.3 | n/a |
| 90 | -42 | 131 | - | - | - |
| 80 | -36 | 113 | 0.458 | 16.3 ± 1.4 | n/a |
| 70 | -31 | 95 | - | 12.1 ± 3.6 | - |
| 60 | -24 | 70 | 0.506 | 7.7 ± 0.5 | -48 |
| 50 | -17 | 39 | - | 4.5 ± 1.1 | -37 |
| 40 | -13 | 21 | 0.692 | 5.7 ± 2.2 | -17 |
| 30 | -11 | 11 | 0.763 | 4.7 ± 0.8 | -26 |
| 20 | -7.5 | 5 | 0.901 | 7.8 ± 0.2 | -24 |
| 10 | -4.5 | 1 | 0.875 | 4.5 ± 0.3 | -15 |
| 0 | -1.2 | 0 | 1.240 | 5.7 ± 0.4 | -19 |

and duty factor were kept at the standard conditions. The lower deposition temperature was used to provide less ideal growth conditions in order to determine the effects of the ion energy. For better comparability here and in the electrical characterizations, film thicknesses were all targeted to be ≈ 550 nm. In Fig. 11 the growth and etch rates are plotted for $V^{rf}_{pp}$ ranging from 0 to 100 V. During each film growth, the $V^{rf}_{pp}$ voltage and the rf power delivered to the stage were kept constant. The variation of the rf-induced dc bias level during the initial stage of the film growth was placed in the Appendix for the interested reader. The measured steady-state rf induced dc bias $< V^{rf}_{pp} >$ and power delivered to the stage for the various $V^{rf}_{pp}$ settings are listed in Table I. Fig. 12 shows the film thickness (in fractional HeNe wavelengths) measured in situ from the reflectometer *vs* time for selected applied $V^{rf}_{pp}$. These reported thicknesses were not compensated for the films' index of refraction and were therefore labeled as 'uncorrected'. From the linearity of this data, the deposition rates were constant the entire growth duration for each individual $V^{rf}_{pp}$ setting.

The FTIR spectra for the corresponding films are given in Fig. 13. Not all spectra are shown and the baselines were offset to show the evolution of peaks more clearly. As noted previously, these spectra represent films that had been removed from the system for more than a week; the film variation with time will be discussed in a future publication. The high energy portion of the spectra (Fig. 13, top) showed the evolution of the broader SiO-H peak at 3450 cm$^{-1}$ as the ion energy

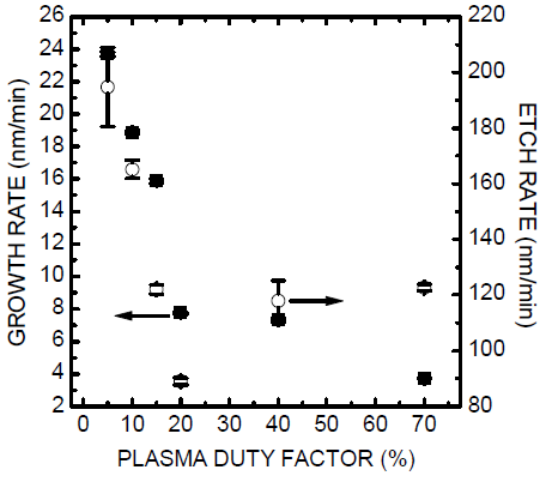


**Fig. 8** Growth (solid) and etch (open) rate variation with plasma duty factor. Duty factor was varied by keeping the e-beam pulse width fixed at 2 ms and changing the period.

decreased. Dotted lines were included to aid the reader on the expanded scale. The lower energy portion of the spectra (Fig. 13, bottom) showed a slight incorporation of the 933 $cm^{-1}$ silanol peak and an HO-H peak at 1600 $cm^{-1}$ as the ion energy decreased.

The root-mean-square (RMS) roughness, breakdown field ($E_{BD}$) and flatband voltage ($V_{FB}$) of the films grown at various $V^{rf}_{pp}$ values are also given in Table I. The index of refraction values from the ellipsometer were erroneous, presumably due to the similar film thickness (550 nm) and laser wavelength (633 nm). The bare Si substrate had a RMS roughness of 0.70 nm. A clear decrease in film roughness was observed as the ion energy was increased, with the final films being smoother than the original substrate when $V^{rf}_{pp}$ exceeded 40 V. The $E_{BD}$ and $V_{FB}$ values increased overall with the incident ion energy, with some fluctuations. The $E_{BD}$ values were consistently above 8 MV/cm when $V^{rf}_{pp} \geq$ 60 V, while the C-V characteristics were more erratic. At the highest ion energies, the C-V characteristics did not represent the standard MOS capacitor model and the determination of the flatband voltage was not available (n/a).

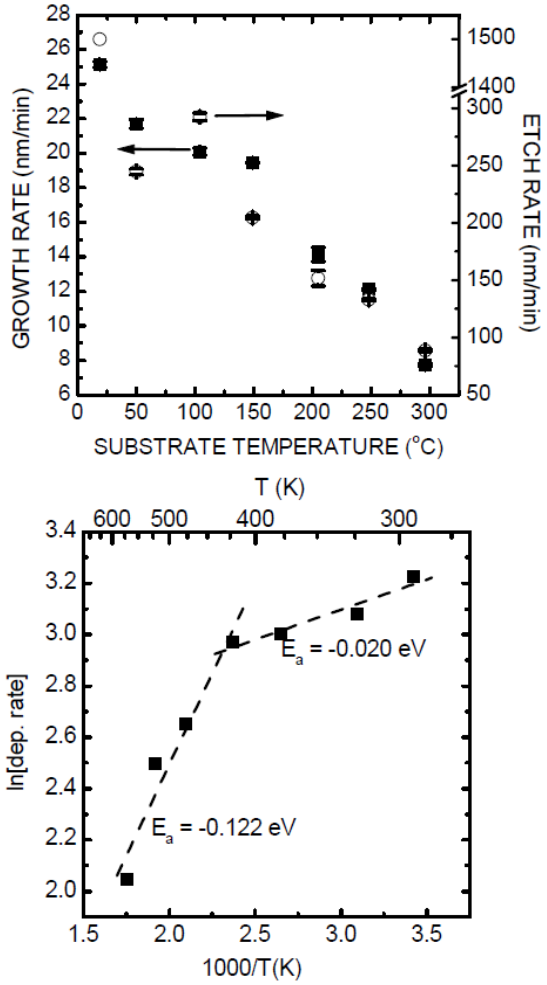


**Fig. 9** (Top) Growth (solid) and etch (open) rate variation with substrate temperature and, (bottom) Arrhenius-type plot of growth rate data. The calculated activation energies ($E_a$) are shown on their respective linear fits.

## IV. DISCUSSION

### A. E-beam generated plasma parameters

Plasmas generated by high energy electron beams have characteristics that make them quite unique when compared to conventional (capacitive, inductively coupled, ECR, microwave or helicon) plasma sources used in materials' processing. The full analytic description of the beam ionization and plasma interaction has been published elsewhere (see Ref. 21), so only a brief review will be given here to assist in the later discussions.

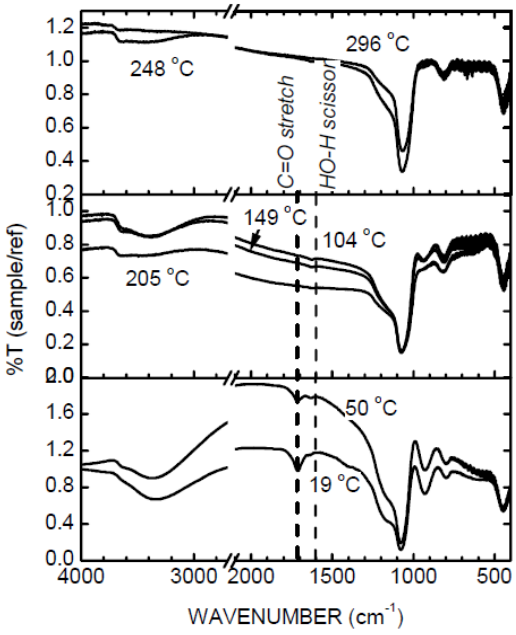


**Fig. 10** FTIR spectra of films grown at various substrates temperatures. Dotted lines mark peak positions discussed in the text.

Instead of heating electrons with externally applied fields to induce and sustain ionization as in conventional plasma sources, the electron beam initiates ionization in this system. The secondary (i.e. plasma) electrons may be created with a wide range of energies, but since no heating mechanisms are applied, the electrons cool rapidly through collisions with the background gas. Hence, higher energy electron-molecule processes (ionization, dissociation) occur first, followed by low energy processes (dissociation, excitation, recombination). The plasma electrons give up all their energy to the gas, effectively 'falling through' all of the available collision processes to the lowest energy process, typically vibrational excitation of the gas. This provides a very cold electron energy distribution that is ~ 0.5 eV when molecular gases are present. The beam energy is typically high enough that only a small percentage is lost as it traverses the system, thereby providing a uniform ionization source over its entire propagation distance. It is important to also point out that operating with a beam energy set at the peak of the ionization cross section (typically ≈ 100 eV) will enhance ionization, but for a gas with an ionization potential of 15 eV the beam energy will be significantly reduced after just a few ionizing events. The reduction of beam energy will significantly decrease the ionization probability and in turn affect the plasma uniformity. Therefore, for high uniformity in the ionization region, it is best to increase the beam energy at the expense of system power.

The single-peaked narrow IEDFs in Fig. 2 illustrate an ion energy control capability unavailable in conventional PECVD systems. The ions exiting the plasma experience the small potential drop across the sheath to the grounded stage. The plasma potential over the course of one period can be considered to be between the most probable and maximum energy of the distribution, or 1.25 to 3.0 Volts. The high energy tail seen in the IEDFs were due to the plasma ignition process that was only present for the first 0.2 ms of the pulse (see Ref. 34). Following the convention set by Lieberman and Lichtenberg [35], the plasma potential can be estimated to be five times the electron temperature, $T_e$, thus $T_e$ = 0.60 to 0.25 eV over the course

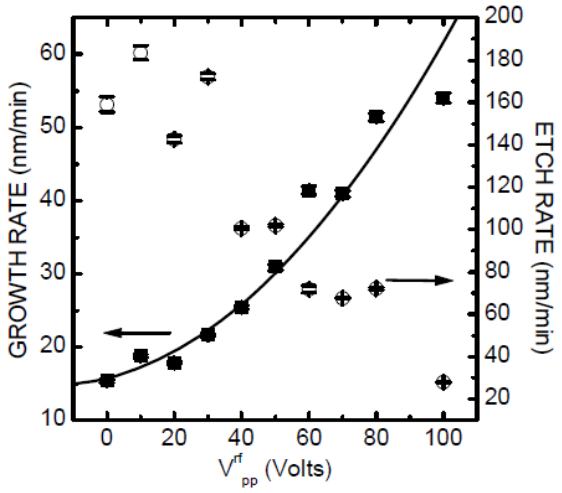


**Fig. 11** Growth (solid) and etch (open) rate variation with applied rf peak-to-peak voltage ($V^{rf}_{pp}$).

of one plasma period. These results agree with previous Langmuir probe measurements (see Ref. 22) in pure oxygen plasmas, as should be expected due to the general electron cooling mechanism discussed above.

Gas-phase collisions are primarily responsible for the flux of plasma species to the substrate. The electron beam will ionize all species since ionization cross sections are all similar at high energies, thus the initial ion composition is heavily tied to the gas composition within the ionization region (beam path). Given the equal flows of argon and oxygen in Fig. 3 (top), one would expect the ionization products to be nearly equal and include both singly and doubly ionized argon species (10:1 ratio) in agreement with the corresponding cross sections and as observed in previous work. However, both species of argon ions can rapidly charge exchange with the abundance of oxygen in the system ($Ar^+ + O_2 \rightarrow Ar + O_{2+}$, k = 5 x $10^{-11}$ $cm^3/s$; $Ar^{+2} + O_2 \rightarrow Ar + 2O^+$, k = 1.4 $10^{-9}$ $cm^3/s$) [36] as well as the atomic oxygen ions ($O^+ + O_2 \rightarrow O + O_2^+$, k = 2 x $10^{-11}$ $cm^3/s$) prior to entering the sampling orifice and subsequently contribute to the dominance of the $O_2^+$ flux at the surface.

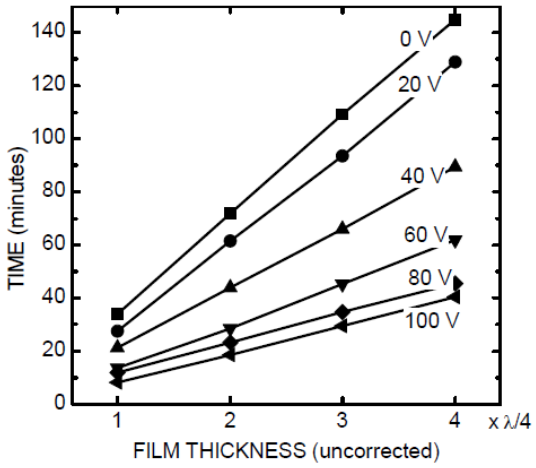


**Fig. 12** Film thickness (in quarter-wavelengths of the 633 nm reflectometer laser) as a function of laboratory time for various $V^{rf}_{pp}$ values.

As discussed previously, the e-beam does not preferentially dissociate molecules with low bond energies; ionization is the dominant interaction, typically resulting in the [larger] daughter ions as seen in standard cross section measurements. Hence, the higher mass region of the ion mass spectra in Fig. 3 resembled the NIST mass spectrum database [37] of TEOS, acquired with an ionizer energy of 70 eV. It is interesting to note the domination of the higher mass peaks by m/q = 60 and 61, identified as $SiO_2^+$ and $SiO_2H^+$, respectively. Given the fact that the mass spectrometer aperture was not heated, it was presumed that these species were not formed in the gas phase but were weakly bonded to the electrode/film and ionized after desorption from the surface. The lower mass portion of the spectra was however dominated by ion-molecule reactions occurring in the gas phase. Most noticeable was the significant depreciation of the $Ar^+$ presence and the increase in the $H_2O/H_3O$ ions. It would be unlikely that these ions were formed by direct reactions with TEOS, since it does not contain any hydroxyl groups (-OH). It is far more likely that these ions were formed by gas phase reactions with the deposition byproduct H2O; since argon ion reactions with water are very rapid ($Ar^+ + H_2O \rightarrow ArH^+ + OH$ or $Ar + H_2O^+$; both with k ≈ $10^{-9}$ $cm^3/s$) as are subsequent reactions with their long-lived products ($ArH^+ + H_2O \rightarrow H_3O^+ + Ar$, $H_2O^+ + H_2O \rightarrow H_3O^+ + OH$; also with k ≈ $10^{-9}$ $cm^3/s$). The other dominant species at m/q = 29 may be from $C_2H_5$, COH or SiH ions. It is unlikely that any silane-based precursors would form, since the final Si-O bond in TEOS is known to form the $SiO_2$ backbone. However, in oxygen-containing mixtures, stable alcohols, hydrocarbons, and aldehydes can be readily formed [38] in the TEOS system at the growth surface. The formation of the stable product $CH_2O$ is reasonable [39], however the absence of the parent m/q = 30 peak ($CH_2O^+$) makes

the presence of the $COH^+$ daughter ion unlikely. The exclusion of these two species imply that the m/q = 29 peak was due to the $C_2H_5^+$ fragment ion or possibly another intermediate source of $COH^+$ (i.e. COH). Since the m/q = 29 peak was not observed in the Ar/TEOS mixture, it was presumed to have been formed through and ion-molecule reaction between an oxygen ion and TEOS, or one of its neutral fragments.

The decrease in the higher mass peaks observed in the neutral mass spectra with the presence of the plasma illustrate the fragmentation of the TEOS molecule by the plasma, as was similarly seen in References 38 - 40. However, unlike these previous studies, the m/q = 2 signal ($H_2^+$) in this work was not a dominant component in the plasma gas, even without oxygen in the gas mixture. The e-beam dissociates the TEOS similar to the mass spectrometer ionizer, however the plasma's low electron temperature and the absence of additional electron heating do not allow additional dissociation the gas fragments. Furthermore, the basic plasma formation mechanisms (e-beam ionization and e-beam dissociation) are not affected by any threshold-energy processes. The plasma electrons are largely low-energy byproducts of beam ionization and any excess energy is removed through collisions with the gas species, in contrast to conventional plasma sources where the applied electrostatic fields continually heat the plasma electrons to maintain the plasma. In such systems, the heating of plasma electrons sustain the lowest threshold-energy processes (ionization and dissociation of large fragment molecules). Hence, instead of completely atomizing the plasma gas larger molecular species are possible in e-beam generated plasmas. In this case, molecular hydrogen, formed primarily by recombination of atomic hydrogen on system walls, will not be prevalent because tremendous amounts of atomic hydrogen were not liberated from the hydrocarbon species.

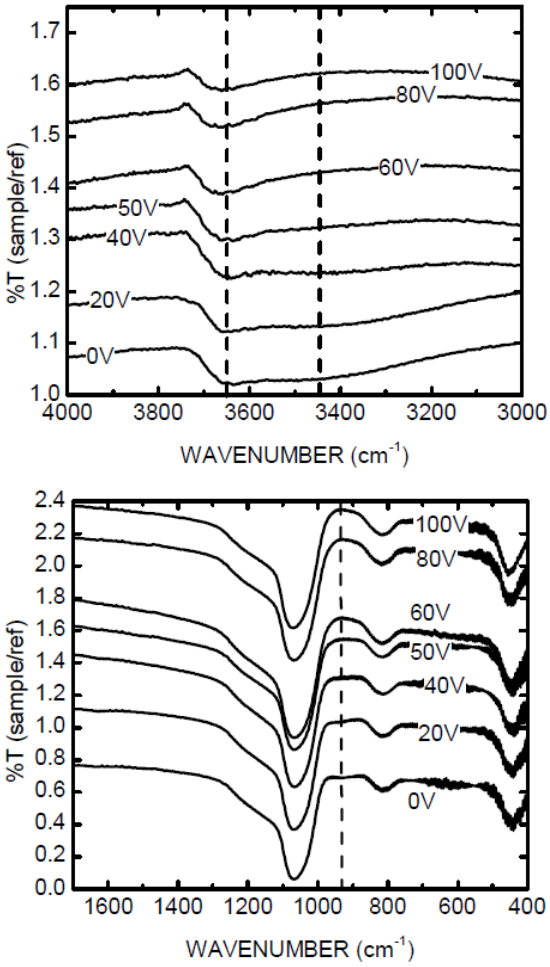


**Fig. 13** FTIR spectra in high energy region (top) and low energy region (bottom) for films grown at various $V^{rf}_{pp}$ values. Dotted lines are drawn for peak location guides as discussed in the text.

With the absence of oxygen in the gas mixture, it would be likely that the neutral species detected were primarily from hydrocarbon species. Thus, the m/q = 26 and 28 species were believed to be from the $C_2H_2^+$ and $C_2H_4^+$ fragment ions of $C_2H_2$ and $C_2H_6$, respectively. However, the other daughter ions from the $C_2H_6$ molecule (m/q = 26, 25, 29, all in comparable abundance) did not show similar changes, and the parent ion (m/q = 30) was not

present. The m/q = 28 peak was therefore identified as $CO^+$ from the CO molecule. The m/q = 78 peak identified as $Si(OH)_3O^+$ is believed to be the de-protonated stable reaction intermediate $Si(OH)_3$, which had been identified by previous authors as the product of SiO and H atoms in the mass spectrometer ionizer, which could also explain the observation of the m/q = 50 peak as $SiH_3OH^+$ as well as the m/q = 56 peak as $SiOC^+$.

The presence of oxygen in the gas mixture enhanced the dissociation of TEOS and the number of reactive radicals in the plasma that arrive at the substrate. Also it would be expected that the hydrocarbon species were rapidly oxidized, as shown in the neutral spectrum, which contained increased amounts typical hydrocarbon oxidation products, namely $H_2O$ ($H_2O^+$ at m/q = 18), CO ($CO^+$ at m/q = 28) and $CO_2$ ($CO_2^+$ at m/q = 44). While the m/q = 28 and 44 peaks can be comprised of additional species ($C_2H_4^+$ and $C_2H_4O^+/SiO^+$, respectively) the increase of these peaks was attributed to the formation of CO and $CO_2$ rather than additional TEOS decomposition products. These identifications are made because the signal change was appreciable when the plasma was present and the peaks were not surrounded by additional daughter peaks. These identifications also agree with those made in Reference 38 in a higher power helicon plasma where appearance potential mass spectrometry was able to be carried out to delineate between the detected species.

## B. Gas composition and duty factor

Silicon dioxide growth from TEOS proceeds by a precursor-mediated adsorption mechanism41 followed by chemisorption/dissociation of the TEOS molecule, presumably by atomic oxygen. Silicon dioxide formation then progresses from these chemisorbed species to a silanol (SiOH) covered surface, which is in turn fully oxidized to form the $SiO_2$ lattice while liberating $H_2O$. Only one of the four Si-O bonds originates from the TEOS molecule and the rest come from the oxygen plasma gas [42]. The observed growth trends at 160 °C and 300 °C in Fig. 4 can be understood from the precursor-mediated adsorption step. As the TEOS flow was increased, precursor material adsorbed on to the substrate more rapidly. However, after this initial physisorbed step, there was insufficient time to form a consistent $SiO_2$ lattice, which resulted in dangling bonds and voids being trapped in the film that allowed the rapid wet etching of the films. At higher surface temperatures, unreacted TEOS molecules and fragments could more readily desorb from the surface, and thereby reduce the frequency of insufficient $SiO_2$ formation. However, even at the elevated temperature of 300 °C the etch rate of the films was large (> 130 nm/min), which implied a high porosity for all cases except for low TEOS flow (≤ 2 sccm) at the higher (300 °C) temperature. The observed decrease of the index of refraction values and breakdown voltage with the increased film porosity was natural [43,44] as the film properties became more like the voids ($n_{air}$ = 1.000) than $SiO_2$ (n = 1.468). The high $E_{BD}$ values (> 8 MV/cm) at low TEOS flows were due to [C-mode] failures intrinsic to the oxide nature. However, the decrease in $E_{BD}$ to 2-8 MV/cm at the higher TEOS flows can be attributed to [B-mode] defects in the oxide. Thus, the films became porous and prone to defects as the TEOS flow was increased. The minor evolution of the SiO-H peaks (3650 and 3450 $cm^{-1}$) and the absence of additional aliphatic peaks in the FTIR data (Fig. 5) suggest that the precursor itself had been nearly fully reacted, but the films were insufficiently bonded into a robust $SiO_2$ lattice. It should be noted that the evolution of these higher energy peaks were somewhat amplified by the spectrum normalization (sample transmission/substrate transmission). The substrates were basically opaque (≈ 0.5 %

transmission) in the higher frequency region, therefore dividing by the substrate spectra accentuated features in this region of the film spectra.

As alluded to earlier, the film composition may have changed upon removal from vacuum, specifically the degree of silanol group formation. The higher energy (3650 $cm^{-1}$) asymmetric peak is due to isolated groups trapped in the film while the lower energy (3450 $cm^{-1}$) symmetric peak arises from a collective interaction between neighboring silanol groups. Thus, both of these peaks can be due to the incomplete oxidation of the films. In addition, strained Si-O-Si bonds can hydrolyze ex situ and form silanol groups, as also seen in silane based chemistry. Typically, *ex situ* hydrolysis would also be accompanied by the incorporation of water peaks in the FTIR spectrum, but it would not be reasonable to rule out either mechanism from these results. However, the presence of the silanol peaks in the 'steady state' films was sufficient to determine and improve the PECVD process viability.
The low growth rate and extremely porous films (high etch rate) when oxygen was removed from the plasma gas mixture in Fig. 6 illustrated the necessity of additional atomic oxygen to react with physisorbed TEOS molecule. From the decreased n value, $E_{BD}$ value and more specifically the top spectrum in Fig. 7, additional oxygen was needed to remove all of the hydrocarbon species from the film as well as create adequate Si-O bonds. Closer examination of the 0% $O_2$ spectrum in Fig. 7 shows not just the additional C-H stretch at 2950 $cm^{-1}$ but also peaks at 1300 and 883 $cm^{-1}$, which have been attributed to $CH_2$ (twist) and the presence of SiH (bend) groups in the film, respectively. With just 10% of the plasma gas comprised of $O_2$, the film growth rate and electrical characteristics improved significantly with a commensurate decrease in the etch rate. Also, the film's chemical composition from FTIR showed no significant contamination, except for the silanol peaks (3650, 3450 and 933 $cm^{-1}$). Above 10% $O_2$ in the gas mixture, the variation of the film properties were subtle and likely not process specific.

The film growth and etch rates showed a shared critical point with the variation of the plasma duty factor (Fig. 8). At the 20% duty factor, the growth rate leveled out as the etch rate minimized, implying that an ideal quasi-steady state for film formation was reached. Since the film growth rates were calculated from the plasma exposure time and higher duty factors did not significantly change the films' characterisitics, the critical time for growth of material at the lower duty factors appeared to be the plasma off time. During the 2 ms plasma exposure time, the substrate would be flooded with reactive oxygen species, with little or no incident energy. When the plasma was turned off the only reactive species in the system becomes atomic oxygen, which diffused through the system as TEOS continued to adsorb on the surface. The diffusive loss rate of the atomic oxygen species through the background gas is given by $K_{loss}$ ($s^{-1}$) $\approx 2D/l_{eff}^2$, where D is the typical diffusion constant and $l_{eff}$ is an effective system length given by the ratio of the chamber volume and surface areas (see Ref. 35, pp. 291-293). The diffusion constant can be written as $\pi\lambda\upsilon_{th}/8$ where $\lambda$ is the mean free path of the O atom and $\upsilon_{th}$ is its thermal velocity. The mean free path is given by the inverse product of the background gas density and collision cross section, thus for the 55 mtorr gas pressure and a collision frequency of $3 \times 10^{-15}$ $cm^2$, $\lambda$ becomes 0.18 cm, resulting in D = 5535 $cm^2/s$ and $K_{loss} = 150$ $s^{-1}$ for a room temperature gas. This loss rate implies that a significant portion of the O atoms have been lost after $\approx$ 7 ms. Thus, for plasma off times less than 7 ms, a significant density of O atoms remain in the system, but for longer times the O atom density has been depleted. For the 20% duty factor case the 8 ms plasma off duration was close to the 7 ms system diffusion time. From the minimum in the etch rate, it appeared that

the modulated plasma could supply sufficient atomic oxygen to react with the constant precursor deposition rate. At lower duty factors, both growth and etch rates were high due to the constant adsorption of TEOS on the surface but the insufficient flux of reactive oxygen prevented the Si-O bonding in to a dense $SiO_2$-like structure. At higher duty factors, the growth and etch rates changed only slightly since the flux of precursor and atomic oxygen remained fairly constant.

## C. Temperature dependence

The decreased growth rate with increased temperature of TEOS-grown $SiO_2$ had been observed previously by other researchers [41,45,46] in low-pressure environments. The higher temperature data in Fig. 9 follows the precursor-mediated adsorption mechanism discussed earlier and described in detail by Deshmukh and Aydil [41]. The key element was that before desorption, the TEOS molecule must find the appropriate bonding configuration in order to dissociate and chemically become part of the film. However, additional energy was necessary to chemisorb and dissociate the TEOS molecule. This additional energy was greater than the energy to desorb the TEOS molecule, giving rise to the [small] negative value for $E_a$. The value of -0.122 eV from these experiments for the temperature range of 150 to 300 °C agrees very well with previous determinations of -0.13 eV (Reference 41, at 165 and 265 °C) and -0.12 eV (Reference 45, for $T \geq 250$ °C).

The Arrhenius-type plot in Fig. 9 however showed two clear $E_a$ values above and below 150 °C. At the lower substrate temperatures TEOS desorbed less rapidly and therefore had more time to find a suitable intermediate bonding configuration, which resulted in a higher film growth rate. The constant flow of TEOS also allowed the substrate surface to be rapidly covered by physisorbed TEOS. The significant decrease in $E_a$ to -0.020 eV at the lower temperature implied that there must be another potential barrier associated with film growth in this system. Others have reported a very similar temperature dependence and attributed it to plasma chemistry changes [47] or prolonged surface migration [48]. However, it is not reasonable to apply either of these mechanisms to the present PECVD system. First, plasma chemistry should not change with the decrease in substrate temperature, unless significantly larger quantities of reactive species (or different species altogether) are being liberated from the surface. Given the large oxygen to TEOS ratio of the present system, it is unlikely that the small substrate will impart any significant change the plasma species. Second, lengthening the surface residence time simply cannot reduce the potential barrier for dissociating of TEOS. The -0.122 eV barrier has been determined as a fundamental limit for film growth, whether it applies specifically to TEOS dissociation or another active surface barrier. If indeed a second reaction pathway to produce $SiO_2$ exists from the gas phase, it should clearly dominate the entire temperature range since it possessed the lower (less negative) activation energy. Therefore, the second regime with the lower activation energy must be the result of a different chemical mechanism on the surface. In other words, a chemically different film was grown. From the FTIR spectra in Fig. 10, much more pronounced O-H peaks appeared as the temperature decreased, from groups of silanols (3450 and 930 $cm^{-1}$) and possibly water (3250 and 1600 $cm^{-1}$), and an additional peak at 1712 $cm^{-1}$ became clear at the lowest temperatures. This additional peak can be attributed to carbonyl groups (C=O) from an intermediate carbonate structure. At high temperatures, this structure thermalyzes and leaves behind Si-O radical sites whereas at lower temperatures it will

hydrolyze and form silanol groups on the film. Thus, below 150 °C a different film was formed that contained not only excessive silanol groups but also the intermediate carbonyl group that did not adequately desorb. The strongly hydrolyzed films in Fig. 10 (and in Fig. 7), can also be formed by *ex situ* hydrolysis, but only the insufficient oxidation of the TEOS can result in the observed second activation energy and inclusion of the carbonyl groups. In light of the given variations in film composition and thickness, the erratic index of refraction measurements were not surprising. Certainly, a more encompassing measurement with a spectroscopic (white-light) ellipsometer could have allowed better consistency among all of the films. However, the films' $E_{BD}$ values did follow the observed composition trend with temperature, going from a defective oxide ($E_{BD} \approx 5$ MV/cm) at low temperatures to a more consistent oxide ($E_{BD} \approx 10$ MV/cm) at the higher deposition temperatures.

**D. Ion energy dependence**

The substrate temperature of 200 °C was chosen to provide a less-than-ideal starting point for the ion energy study. After the rearrangement of the TEOS gas feed, the growth rates remained consistent with the previous temperature study data, which should be expected for a well-mixed gas system. The growth rate increase with ion energy in Fig. 11 was unexpected. The previous growth rates of the films (10-15 nm/min) were reasonable for a non-optimized research tool, but the inclusion of ion energy increased the deposition rate (50-60 nm/min) to that of a highly competitive commercial process. The coincident decrease in etch rate implied that the additional ion energy densified the films as expected and the increasing growth rate implied that the ion bombardment accelerated the removal of reaction by products. At these low ion energies (maximum of 47 eV from Table 1) sputtering yields for $SiO_2$ are low, hence there should be no competition with the growth rate, corroborating the in situ reflectometry observations that no etching took place even during the post-treatment phase.

The linearity of the film thickness with deposition time (Fig. 12) demonstrated highly consistent growth conditions throughout the film formation. Conversely, if the ion energies had changed during the deposition as implied by the voltage probe measurement of $\langle V^{rf}_{pp} \rangle$, the dependencies in Fig. 12 would be erratic and highly non-linear, which was not the case. Thus, it was reasonable to assume that the ion energies were at their steady state values given in Table 1 throughout the film growths.

The FTIR spectra in Fig. 13 accentuate the important role of the ion energy in PECVD at lower temperatures. As the ion energy decreased, the occurrence of isolated silanol groups (illustrated by the asymmetric peak at 3650 $cm^{-1}$) became more pronounced and eventually gave rise to the symmetric silanol peak at 3450 $cm^{-1}$ from neighboring group interactions. The lesser silanol peak at 933 $cm^{-1}$ was however barely visible, compared to the previous temperature study (see Fig. 10). In these films of very similar thicknesses, no discernable peak broadening or shifting could be seen in these spectra, although it should be noted that the FWHM of the Si-O-Si stretch was 75 to 80 $cm^{-1}$, in agreement with other work that identified dense $SiO_2$ structures with 85 $cm^{-1}$ peak widths for the 1080 $cm^{-1}$ peak. From these spectra, ion energies above 17 eV ($V^{rf}_{pp} = 50$ V) created dense films that do not readily form or convert to large concentrations of silanol groups.

The ion energy limit associated with the $V^{rf}_{pp} > 50$ V was also observed in the films' electrical properties. The $E_{BD}$ values in Table 1 were only dominated by the intrinsic nature

of the oxide ($E_{BD}$ > 8 MV/cm) while lower ion energies produced films that failed due to actual film defects ($E_{BD}$ = 2-8 MV/cm). The trend in the flatband voltages for the MOS capacitor structures further pinpointed the film-growth damage issue. The generally observed trend in the C-V characteristics and increasing $V_{FB}$ shift implied that the film defects were due to mobile charges or charge injection. Above $V^{rf}_{pp}$ = 60 V a consistent measurement of $V_{FB}$ could not be obtained, likely because the devices had become dominated by a high level of interface trap densities. The large interface trap density would have been incorporated by damage of the silicon surface at the earlier stages of deposition. (It should also be pointed out that these films were purposely never annealed or exposed to forming gas treatments to improve their electrical characteristics in order to maintain a complete 'low temperature' PECVD process.) Thus, a lower initial ion energy would necessary to prevent severe interface trap densities, but then ion energy could be increased to promote film growth and density.

Film morphology was consistently improved with the increased ion energy. The selected RMS roughness data in Table I show that ion energies above 13 eV (40 $V^{rf}_{pp}$) kept the surface morphology consistent with the original substrate. This ion energy is quite low, below the ion energy capable of many conventional discharges using a grounded substrate, due to their higher plasma potentials. Thus, a lower limit to the ion energy can be tied to the film roughness. Another fundamental limit can be determined by estimating the average of energy deposited per $SiO_2$ molecule. In general, films are preferentially deposited under low (10-30 eV) or intermediate (~ 100 eV) ion energies, sufficient for densification but using high ion fluxes ($\Phi$i). [1,49] This deposition energy is defined as $E_d = E_i(\Phi_i/\Phi_c)$, where $E_i$ and $\Phi_i$ are the ion energy and flux, respectively, and $\Phi_c$ is the flux of condensing units that can be estimated by the film growth rate and density of $SiO_2$ (2.2 g/cm$^3$). In these experiments, the ion flux to the stage was estimated to be 4.4 x $10^{-6}$ ions/s/cm$^2$. From Fig. 11, an average growth rate of 30 nm/min was observed, which estimates a condensing particle flux of 1.1 x $10^{15}$ molecules/s/cm$^2$. Thus, $E_d$ = 3.6 $E_i$, which means that the energy deposited per $SiO_2$ molecule was significantly higher than the incident ion energy for the 200 °C PECVD process in these experiments. From the discussions of Figs. 11 and 13, there were significant changes in the film character when $V^{rf}_{pp}$ exceeded 50 V. The corresponding ion energy (17 eV) results in an $E_d$ value of 51 eV. This $E_d$ value agrees with the results from Ref. 49 that deposited $SiO_2$ films via e-beam evaporation with ion-assist provided by an independent ion gun. In that work, an increase in the density of the silica matrix was seen as $E_d$ values increased from 20 to 50 eV, and ion-assisted samples where $E_d$ < 50 eV demonstrated an instability after exposure to laboratory air. However, comparing these e-beam evaporated film results to the present PECVD experiments may lead to irresolvable differences. In this modulated PECVD system, steady-state quantities such as flux and ion energy were estimated and not fully treated for temporal variations. This is actually true of most PECVD systems, as ion energies are considered to be single-valued and, when modulated, variation of global plasma parameters are difficult to determine. In addition, the evaporation/ion-assist films were carried out at UHV conditions with reduced film growth chemistries. Thus the results complement one another in determining the role of ion energy in $SiO_2$ film growth in PECVD and physical vapor deposition (PVD) systems.

## V. SUMMARY

A low pressure PECVD process for the growth of $SiO_2$-like films using a modulated electron-beam generated plasma was investigated in terms of the plasma constituents, process variables and the final properties of the resultant steady-state films. Mixtures of TEOS, argon and oxygen (2:48:50, typically) were used to produce plasmas with very low ion energies (< 3 eV) and a diverse control over processing parameters. Energy-resolved mass spectrometry illustrated the low energies of the plasma ions, as well as the ion-chemistry changes in the growth gas mixture. At typical growth conditions, water byproduct from the film result in water-based ions ($H_2O^+$/ $H_3O^+$) that became major plasma constituents. Measurements of neutral species showed that while TEOS was dissociated in the plasma, typical small molecules ($H_2$, $CH_2O$) were not formed in abundance due to the less aggressive nature of the e-beam generated plasma. Since the plasma electrons are not constantly energized to sustain the plasma, severe fragmentation and eventual atomization of constituents is avoided. However, reaction byproducts ($H_2O$, CO, $CO_2$) become significant gas phase constituents.
Films formed at a large oxygen-to-TEOS ratio (> 10:1) proceeded through a precursor-mediated growth mechanism, as evidenced by a small negative activation energy of -0.122 eV. Also, the presence of a second smaller activation energy (-0.020 eV) in a lower temperature regime ($T \leq 150$ °C) illustrated the formation of an $SiO_xC_yH_z$ film, that has not been typically seen in other PECVD systems. By judicious modulation of only the plasma generation source, the system's diffusion time was seen to continuously deliver sufficient atomic oxygen species to react with the continuously-fed silanorganic precursor. Perhaps most importantly, film contamination by hydrocarbon species was only observed when no additional oxygen was added to the system.

The role of ion energy was explored in terms of the deposition rate, porosity, chemical stability, electrical characteristics and roughness of the final film. While the use of an electron-beam generated system introduced some subtle complexities, the high degree of control of the ion energy and consistent growth rates of 10 to over 50 nm/min provided a significant advancement in the low temperature $SiO_2$ film growth for numerous applications. A lower ion energy limit of 14-17 eV was necessary to produce films of reasonable chemical quality and smoothness. This condition corresponded to 51 eV being deposited per condensing unit of $SiO_2$ in the low ion flux regime. From the present data, no clear upper limit of the ion energy was observed (up to incident ion energies of 47 eV) on the film growth rate, although significant changes in the films' electrical properties were seen. Defects due to mobile charges or charge injection in the films' were observed, which increased with the incident ion energies. For $V^{rf}_{pp} \geq 50$ V (17 eV), the flatband voltages of MOS capacitors were excessive (> 35 V) for the as-processed films, until a large interface trap density dominated at ion energies above 31 eV. The determination of these (and lower) ion energies is prohibited by most plasma systems due to their larger plasma potentials. The evolution of films from vacuum will be discussed in a subsequent publication.

## VI. CONCLUSION

Electron beam generated plasmas have shown great promise in a PECVD process that comprised of fairly complicated chemistries. The tunability of the ion energy from extremely low values unattainable in conventional plasmas makes the system attractive for many

PECVD processes. In the TEOS/$SiO_2$ system presented here, a specific set of process parameters (gas flows, temperature) were established, as well as additional global parameters (duty factor, incident ion energy) that can be considered for other systems. In this system, film contamination by hydrocarbon was not an issue presumably due to the lack of constant gas dissociation. From these results, an ideal system parameters for low temperature deposition would be TEOS/Ar/$O_2$ flows of 1:49:50, respectively, a duty factor $\geq$ 50% and a variable ion energy, starting around 17 eV to reduce interface trap formation then increasing to above 31 eV to produce smooth, dense, stable films of high chemical purity. The requirement of continuous plasma generation was not necessary as long as atomic oxygen species do not diffuse out of the system too rapidly, which can be used to reduce the total input power of the system. With the very low initial ion energies and widely variable flux capabilities, this system was able to access a full range of chemical process space and enable a better understanding of the growth of $SiO_2$ films from TEOS and perhaps other precursors. From this work, other chemistries (hexamethyl disiloxane, tetramethyl silane) and films (amorphous Si:H, SiN) can also be addressed.

## ACKNOWLEDGEMENTS

The authors gratefully the assistance of Dr. John Russell (NRL) for the generous use of his FTIR spectrometer, Drs. Richard Fernsler and Charles Eddy, Jr., (NRL) for their always insightful discussions, Ms. Lauren Haspert of SFA Inc. (Largo, MD) for growing a significant number of the films, Mr. Bryan Orf for the AFM measurements and Mr. Marko Tadjer for the CV measurements (both from the University of Maryland). This work was supported by the Office of Naval Research.

## APPENDIX

The rf-induced, dc bias level $<V^{rf}_{pp}>$ measured by the oscilloscope probe changed significantly during the earlier stages of the film growths. Initially, dc voltage levels were large negative values (-20 to -70 V) during the pulse with an overall baseline offset of approximately -20 V. As the films grew, the magnitude of the dc voltage levels decreased, until the $<V^{rf}_{pp}>$ during the pulse was approximately one-half the applied rf voltage and the baseline offset was zero. The film thicknesses (from the *in situ* reflectometer) were approximately 325 nm when the dc voltage signals reached these conditions. The discrepancy between these largely varying voltage probe measurement of the stage potential during deposition and the obvious linear growth rates require additional analysis of the overall plasma system operation.

At first glance, one would assume that the voltage probe measurement was inaccurate, although after a certain film thickness ($\approx$ 300 nm) was grown, the measurements appeared reasonable ($V_{bias} = V^{rf}_{pp}/2$). These observations can be explained in the following way: In all plasma systems, the plasma currents must leave the system at the same rate, regardless of wall conditions. However the injected e-beam current in this system cannot be balanced by plasma currents. In the oxide-coated chamber the e-beam terminated at the insulated chamber wall and could penetrate up to 80 nm given the beam energy and accepted density of $SiO_2$. Thus, the beam current becomes embedded in the wall dielectric and builds

up a negative charge density, $\sigma_s$. This charge density can in turn drive the plasma potential negative to $\sigma_s d/4\varepsilon$, where d is the mean depth of charge and $\varepsilon$ is the dielectric strength of $SiO_2$. For the pulsed e-beam, we expect a beam current of ~ 5 $A/m^2$, which gives a charge density of 0.01 $C/m^2$ for each pulse. Thus, with $4\varepsilon \approx 3.5 \times 10^{-11}$ F/m, each pulse could cause a – 20 V decrease in the plasma potential. Depending on the rate at which this built up charge can bleed off, successive pulses could easily cause the plasma potential to the large negative values measured here. These large negative values are however referenced to ground, but the stage floats due to the blocking capacitor in the rf network. Thus the surface only sees the 'typical' plasma potential of a few volts. Once the sample became covered with insulating film, it was electrically a larger capacitor ($C_{film} = \varepsilon A/d \approx 30$ nF, for a 300 nm $SiO_2$ film) on top the rf blocking capacitor (~ 1 nF), which in turn completely blocked the dc effects of the e-beam on the plasma potential in the insulated chamber.

**References**


[1] L. Martinu and D. Poitras, J. Vac. Sci. Technol. A 18 (6), 2619 (2000).

[2] A.M. Mahajan, L.S. Patil, J.P Bange, and D.K. Gautam, Surf. Coat. Technol., 183, 295 (2004).

[3] M. Creatore, "Plasmas, Polymers and Plasma-deposited Polymer-like Films: Plasma Diagnostic Studies for SiO2-like Film Deposition," at The AVS 51st International Symposium, 14-19 November 2004.

[4] Granier, C. Vallée, A. Goullet, K. Aumaile, and G. Turban, J. Vac. Sci. Technol. A 17, 2470 (1999).

[5] E.D. van Hattum, "In-Situ Characterization of Radiofrequency Magnetron Sputter Deposition of SiOx using Elastic Recoil Detection," at The International Conference on Metallurgical Coatings and Thin Films, 2-6 May 2005, San Diego, CA.

[6] Lefèvre, L.J. Lewis, L. Martinu, and M.R. Wertheimer, Phys. Rev. B 64, 115429 (2001).

[7] D. Leonhardt and S.G. Walton, submitted to Plasma Sources and Science Technology.

[8] Flexible Microelectronics and Displays Conference, USDC Conference Proceedings, 1-3 February 2005, Phoenix, AZ.

[9] P.I. Hsu, R. Bhattacharya, H. Gleskova, M. Huang, Z. Xi, Z. Suo, S. Wagner, and J.C. Sturm, Appl. Phys. Lett., 81 (9), 1723 (2002).

[10] Sazonov, A. Nathan, and D. Striakhilev, J. Non-Cryst. Solids 266-269, 1329 (2000).

[11] K.R. Sarma, C. Chanley, S. Dodd, J. Roush, J. Schmidt, G. Srdanov, M. Stevenson, G. Yu, R. Wessel, J. Innocenzo, M. O'Regan, W. A. MacDonald, R.Eveson, K. Long, H. Gleskova, S. Wagner, J. C. Sturm, in Cockpit Displays X, Ed. D. G. Hopper, Proceedings of the SPIE, edited by D.G. Hopper, Vol. 5080, (2003), pp. 180-191.

[12] H. Gleskova, S. Wagner, V. Gašparík, and P. Kováč, J. Electrochem. Soc. 148 (7) G370 (2001).

[13] Madan, Surf. Coat. Technol. 200, 1907 (2005).

[14] M.R. Pinnel, "Overview of Flexible Display Technology: Why, What and When?" at the US Display Consortium on Plastic Electronics, 4 October 2005. See http://www.usdc.org/resources/tutorials/Overview_Flex_Tech_Oct2005.pdf.

[15] L. Martinu and R.P. Shimshock, Vacuum Tech. & Coat. 4(2) 20 (March 2003).

[16] L.R. Thompson, J.J. Rocca, J.D. K. Emery, P.K. Boyer, and G.J. Collins, Appl. Phys. Lett. 43 (8), 777 (1983).
[17] J.J. Rocca, J.D. Meyer, M.R. Farrell, and G.J. Collins, J. Appl. Phys. 56 (3) 790 (1984).
[18] K.D. Schatz and D.N. Ruzic, Plasma Sources Sci. Technol. 2, 100 (1993).
[19] M.J. Kushner, W. Z. Collison, and D.N. Ruzic, J. Vac. Sci. Technol. A 14 (4) 2094 (1996).
[20] R.A. Meger, R.F. Fernsler, M. Lampe, and W. Manheimer, US Patent # 5,874,807.
[21] R.F. Fernsler, W.M. Manheimer, R.A. Meger, J. Mathew, D.P. Murphy, R.E. Pechacek, and J.A. Gregor, Physics of Plasmas 5 (5) 2137 (1998).
[22] D. Leonhardt, S.G. Walton, D.D. Blackwell, W.E. Amatucci, D.P. Murphy, R.F. Fernsler, and R.A. Meger, J. Vac. Sci. Technol. A 19 (4) 1367 (2001).
[23] S.G. Walton, D. Leonhardt, D.D. Blackwell, R.F. Fernsler, D.P. Murphy, and R.A. Meger, J. Vac. Sci. Technol. A 19 (4) 1325 (2001).
[24] C. Muratore, S.G. Walton, D. Leonhardt, R.F. Fernsler, D.D. Blackwell, and R.A. Meger, J. Vac. Sci. Technol. A 22 (4) 1530 (2004).
[25] D. Leonhardt, C. Muratore, and S. G. Walton, IEEE Trans. Plasma Sci. 33(2), 783 (2005).
[26] S.G. Walton, C. Muratore, D. Leonhardt, R.F. Fernsler, D.D. Blackwell and R.A. Meger, Surf. Coat. Technol. 186 (1-2), 40 (2004).
[27] D. Leonhardt, S.G. Walton, C. Muratore, R.F. Fernsler, and R.A. Meger, J. Vac. Sci. Technol. A 22 (4) 2276 (2004).
[28] J.A. Theil, D.V. Tsu, M.W Watkins, S.S. Kim, and G. Lucovsky, J. Vac. Sci. Technol. A 8(3), 1374 (1990).
[29] D. Souch, A. Brunet-Bruneau, S. Fisson, V. Nguyen Van, G. Vuye, F. Abeles, and J. Rivory, Thin Solid Films 313-314, 676 (1998).
[30] J. Batey & E. Tierney, J. Appl. Phys. 60 (3), 3136 (1988).
[31] D. K. Schroder, Semiconductor Material and Device Characterizations, 3rd ed., (Wiley, New Jersey, 2006), Chapter 6.
[32] S.G. Walton, D. Leonhardt, and C. Muratore, IEEE Trans. Plasma Sci. 33(2), 838 (2005).
[33] Brunet-Bruneau, J. Rivory, B. Rafin, J.Y. Robis, and P. Chanton, J. Appl. Phys. 82 (3) 1330 (1997) and the references therein.
[34] S.G. Walton, D. Leonhardt, D.D. Blackwell, D.P. Murphy, R.F. Fernsler, and R.A. Meger, Phys. Rev. E 65, 046412 (2002).
[35] M.A. Leiberman and A.J. Lichtenberg, Principles of Plasma Discharges and Materials Processing, (Wiley, New York, 1994), p. 161.
[36] Y. Ikezoe, S. Matsuoka, M. Takebe, and A. Viggiano, Gas Phase Ion-Molecule Reaction Rate Constants Through 1986, (Ion Reaction Research Group, Tokyo, 1987).
[37] NIST Mass Spectral Database, NIST Chemistry WebBook, NIST Standard Reference Database Number 69, (June 2005 release). See http://webbook.nist.gov/chemistry/.
[38] K. Aumaille, A. Grainer, M. Schmidt, B. Grolleau, C. Vallée, and G. Turban, Plasma Sources Sci. Technol. 9, 331 (2000).
[39] C. Charles, P. Garcia, B. Grolleau, and G. Turban, J. Vac. Sci. Technol. A 10 (4), 1407 (1992).

[40] K. Okimura and N. Maeda, J. Vac. Sci. Technol. A 16 (6), 3157 (1998).
[41] S.C. Deshmukh and E.S. Aydil, J. Vac. Sci. and Technol. A 13 (5), 2355 (1995).
[42] N. Selamoglu, J.A. Mucha, D.E. Ibbotson, and D.L. Flamm, J. Vac. Sci. Technol. 7(6), 1345 (1989).
[43] N. Benissad, C. Boisse-Laporte, C. Valleé, A. Granier, and A. Goullet, Surf. Coat. Technol. 116-119, 868 (1999).
[44] K. Aumaille, C. Valleé, A. Granier, A. Goullet, F. Gaborian, and G. Turban, Thin Solid Films 359, 188 (2000).
[45] C.S. Pai and C.P. Cheng, J. Appl. Phys. 68 (2), 793 (1990).
[46] F. Fracassi, R. d'Agostino, and P. Favia, J. Electrochem. Soc. 139 (9), 2636 (1992).
[47] W. Kulisch, T. Lipmann, and R. Kassing, Thin Solid Films 174, 57 (1989).
[48] K. Sano, H. Tamamaki, M. Nomura, S. Wickramanayaka, Y. Nakanishi, and Y. Hatanaka, in MRS Symposia Proceedings, vol. 396, (1996), pp. 539.
[49] Brunet-Bruneau, D. Souche, S. Fisson, V. Nguyen Van, G. Vuye, F. Abeles, and J. Rivory, J. Vac. Sci. Technol. A 16 (4), 2281 (1998).